Optical property of nanocomposite of mesoporous silica thin films incorporated with gold nanoparticles

Jingyue Fang (方靖岳)[1*], Xueao Zhang (张学骜)[2], Shiqiao Qin (秦石乔)[2], and Shengli Chang (常胜利)[2]

[1] *College of Optoelectric Science and Technology, National University of Defense Technology, Changsha 410073, China*

[2] *College of Science, National University of Defense Technology, Changsha 410073, China*

[*] *Corresponding author: fjy_nudt@yahoo.com.cn*

Received August 24, 2010; accepted November 15, 2010; posted online February 21, 2011

Amino-functionalized mesoporous silica thin films (MTFs) are produced using surface active agent F127, and then gold nanoparticles are introduced into the pore channels to prepare the Au/SiO_2 nanocomposite. After assembling the gold, the amino-functionalized MTF undergoes some shrinkage but remains a periodic structure as demonstrated by X-ray diffraction (XRD) patterns. The nanocomposite shows an acute characteristic diffraction peak assigned to (111) plane of the face-centered-cubic structure of gold, indicating that gold nanoparticles crystallize well and grow in a preferred orientation in the pore channels. The surface plasma resonance (SPR) absorption peak near 570 nm undergoes a red-shift accompanied by a strengthening of intensity when $HAuCl_4$ is used to react with the amino groups on the internal pore surfaces for 4, 6, and 8 h. The simulative results are consistent with the experimental ones shows that the absorption property of the Au/SiO_2 nanocomposite is influenced by the dipping time, which affects the size and volume fraction of embedded gold nanoparticles.

OCIS codes: 240.0310, 310.6860, 240.6680.

doi: 10.3788/COL201109.032401.

Nanofabrication includes two approaches: the top-down approach with ultrahigh resolution, developed from optical lithography, and the bottom-up approach using biochemical effects to recombine or assemble molecules or atoms. Both electron beam lithography (EBL) and ion beam lithography (IBL) transfer patterns to substrates via high energy beams[1−4], while scanning probe optical lithography (SPOL) draws support from the effects of tunneling current, mechanical force, or near-field optical wave existing between the probe and sample to carve patterns[5−8]. EBL, IBL, and SPOL are top-down technologies. Using materials with a periodic array of islands or holes as templates, and using ordered physical processes or chemical reactions to structure nanomaterials are called bottom-up methods[9−11]. Solid porous matrices such as mesoporous silica thin films (MTFs) have large surface areas (up to ca. 1500 m^2/g), high pore volumes (up to ca. 1.5 cm^3/g), uniform nanopores of tunable sizes (2 − 50 nm), different shapes (cylindrical and cage-like), and mesostructures, thereby providing considerable opportunities in the synthesis of nanostructural materials. Because the pore size of MTF can be controlled using different surfactants, they can be used as templates for the synthesis of metallic nanoparticles with controlled size and morphology. To date, the fabrication of MTFs incorporated with gold nanoparticles have been reported by some groups[12−14]. However, few studies have been conducted to analyze the nanocomposite's optical properties influenced by the size and volume fraction of the embedded gold nanoparticles.

Recently, optical properties based mainly on the surface plasma resonance (SPR) of noble metal particles have attracted considerable interest because of their potential uses in a wide range of technological applications[10,15,16]. Here, we present the preparation of a Au/SiO_2 nanocomposite by the down-up route, and analyze how dipping time influences the SPR absorption properties of the Au/SiO_2 nanocomposite.

The functionalized silica films were deposited on a glass substrate by co-condensation of tetraethoxysilane (TEOS) and 3-aminopropyltriethoxysilane (APTES) in the presence of Pluronic $EO_{106}PO_{70}EO_{106}$ (F127) under acidic conditions. In the synthesis, TEOS (98%, Aldrich), ethanol, deionized water, and dilute HCl (0.1 mol) were refluxed at 60 °C for 1 h. The solution was cooled to room temperature and diluted with ethanol followed by further addition of deionized water and concentrated HCl (37%). To this solution, APTES (99%, Acros) was added slowly with vigorous stirring at 0 °C. Finally, F127 was dissolved in ethanol and added to the prehydrolyzed solution. The final reactant molar ratios were: 0.9 TEOS: 0.1 APTES: 0.15 HCl: 20 C_2H_5OH: 5 H_2O: 0.006 F127. The final solution was stirred for 1 h prior to dip-coating on glass substrates at the withdrawing rate of 16 cm/min. After the as-deposited thin films were dried in air at ambient temperature for 24 h, they were heat-treated in air at 120 °C for 24 h and complete siloxane condensation. The F127 surfactant was removed from the thin films by extraction with hot ethanol under reflux for 24 h, and the amino-functionalized MTFs with open pore structures were obtained[17,18].

A standard $HAuCl_4$ solution with a concentration of 0.05 mol was prepared by dissolving $HAuCl_4{\cdot}4H_2O$ powder with deionized water. The three pieces of glass that deposited functionalized mesoporous silica films were placed in the $HAuCl_4$ solution for 4, 6, and 8 h, respectively, followed by rinsing with water for 5 min. The samples were rinsed with deionized water and dried in

air for 24 h. After this, the samples were placed in the muffle furnace at 450 °C for 4 h, increasing the temperature from ambient temperature at a rate of 1 °C/min. Finally, the samples were cooled to room temperature and the Au/SiO_2 nanocomposites were obtained[13].

X-ray diffraction (XRD) patterns were obtained using a Rigaku D/MAX2200 diffractometer featuring Cu Ka radiation ($\lambda = 0.15418$ nm) at 40 kV and 200 mA. Transmission electron microscope (TEM) and high resolution transmission electron microscope (HRTEM) images were recorded with a FEI Tecnal G^2 20 S-Twin apparatus at an accelerating voltage of 200 kV. For TEM observations of the nanocomposite, the film loaded with gold was peeled from the glass wafer in ethanol and the supernatant solution was deposited on a copper microgrid. For TEM observations of the dispersed gold nanoparticles, the Au/SiO_2 nanocomposite peeled from the glass substrate was placed in a solution of HF/ethanol, which dissolved the silica frameworks. Alkanethiols were added as stabilizing ligands, and then the separative gold nanoparticles were obtained. Ultraviolet(UV)-visible absorption spectra were recorded on a HITACHI U-4100 spectrometer. The morphology of an extracted MTF was observed by TEM as shown in Fig. 1, which illustrates well-ordered mesoporous structures.

Figure 2(a) shows the XRD patterns of amino-functionalized MTFs aged for different periods and followed with ethanol extractions for 24 h. The intense diffraction peaks can be observed at about $2\theta = 1.0°$, indexed to (200) reflections of a three-dimensional (3D) Im3m cubic symmetry. The small-angle XRD pattern peaks can be found after the incorporation of gold nanoparticles, but undergoes a big-angle-shift, as shown in Fig. 2(b). This indicates that the Au/SiO_2 nanocomposite framework remains a periodic structure but the silica frameworks exhibit contraction. Using anhydrous ethanol to extract the surface active agent is a suitable approach, which will not destroy the amino groups and the structure of the matrix. The following calcination procedure was implemented at 450 °C, which should not be too high; otherwise, an intense shrinkage of the mesoporous films will occur and can even destroy the structure.

Figure 3 presents the wide-angle XRD pattern of the gold-nanoparticle-loaded MTF. The peak of the Au/SiO_2 nanocomposite at about $2\theta = 24°$ is produced by the glass substrate, and the intense diffraction peak at about 2θ = 38.18°, indexed as (111) plane, is characteristic of a face-centered-cubic structure of gold with a d-spacing of 0.23 nm. This indicates that gold has crystallized well in the pore channels. That the intensities of characteristic diffraction peaks at $2\theta = 44.39°$ and 64.57°, assigned to (200) and (220) planes of the gold, are very weak and the absence of any other characteristic diffraction peak indicates that gold is selectively grown in the pore channels along (111) plane.

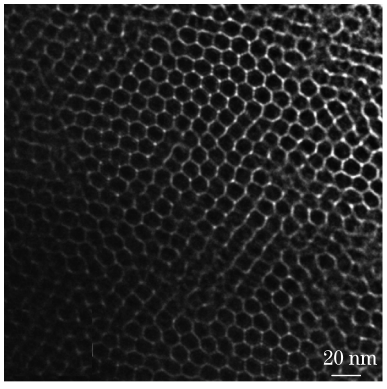

Fig. 1. TEM image of an extracted amino-functionalized MTF.

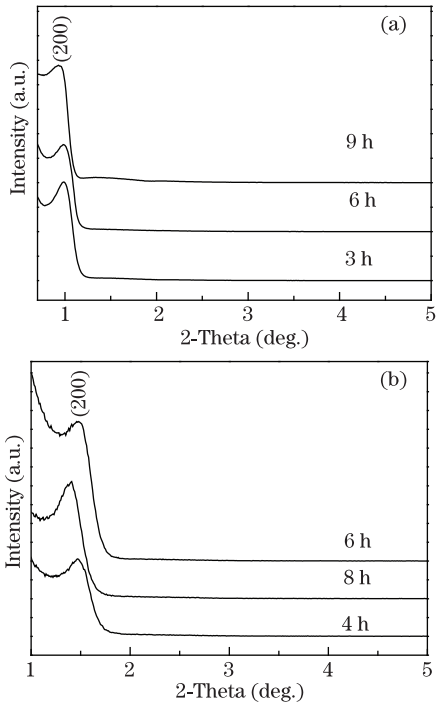

Fig. 2. Small-angle XRD patterns of amino-functionalized MTF from TEOS:APTES:F127 = 0.9:0.1:0.006 sol (a) at different aging times followed with ethanol extractions for 24 h to remove the surfactant; (b) incorporated with gold for different dipping periods in an ethanol solution of $HAuCl_4{\cdot}4H_2O$ after aging for 3 h and extraction for 24 h.

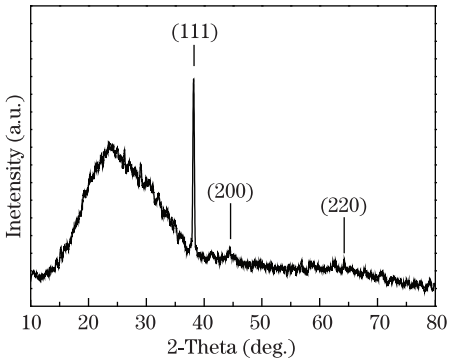

Fig. 3. Wide-angle XRD pattern of Au/SiO_2 nanocomposite dipped in $HAuCl_4$ solution for 4 h.

The amino-functionalized MTF is alkalescent, $HAuCl_4$ can be introduced into pore channels by a neutralization reaction, and gold element exists in the inner surface of pore channels in the form of $AuCl_4^-$ salt[14]. Followed by a calcinations procedure at 450 °C, $AuCl_4^-$ salt breaks down into Au, HCl, Cl_2, etc., and Au crystallized more efficiently because of the annealing. Thus, the characteristic diffraction peak assigned to (111) plane

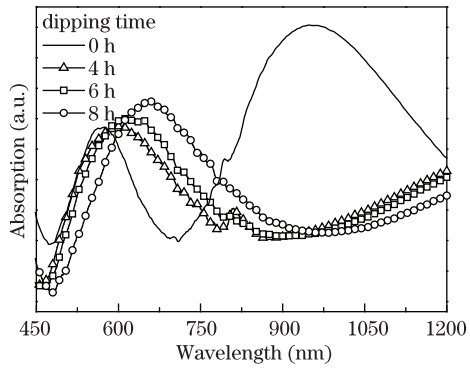

Fig. 4. UV-visible spectra of Au/SiO_2 nanocomposites dipped for 0, 4, 6, and 8 h in an ethanol solution of $HAuCl_4{\cdot}4H_2O$.

of gold can be observed. The immobilization of gold on amino-functionalized MTF depends on weak interaction between different molecules, and atoms self-assemble into regular structures, which decides whether gold is loaded in accordance with a certain law and is demonstrated as a selective-growth in the pore channels along (111) planes[14].

Figure 4 shows the optical absorption spectra of the MTFs, which were loaded with gold for different dipping times, measured with a HITACHI U-4100 spectrometer using a wolfram lamp in the range from 450 to 1200 nm. As shown in Fig. 4, the MTF without gold nanoparticles shows two intense absorption peaks, located at about 570 and 950 nm. After gold was incorporated into the pore channels of the MTFs, the absorption spectra obviously differs. The absorption peak near 950 nm disappears (shifts to a location of more than 1200 nm), and the peak near 570 nm undergoes a red shift to approximately 600, 620, and 650 nm after dipping in $HAuCl_4$ solution for 4, 6, and 8 h, respectively. Meanwhile, the intensity of absorption peaks is strengthened and the width of absorption peaks is slightly widened as the dipping time is extended. As shown in Figs. 5(a)–(c), the gold nanoparticles are extracted by dissolving the silica frameworks of Au/SiO_2 nanocomposites with a solution of HF/ethanol, and then using dodecane-1-thiol ($C_{12}H_{25}SH$) as stabilizing ligands[13]. The gold nanoparticles are formed almost in the shape of spheres. Figures 5(d)–(f) show the particle size distributions of the gold nanoparticles shown in Figs. 5(a)–(c), respectively. The size of the gold nanoparticles ranges from 5.2 to 8.3 nm, and the mean size is about 6.8 nm in Fig. 5(a); the size of the gold nanoparticles ranges from 5.0 to 14.0 nm,

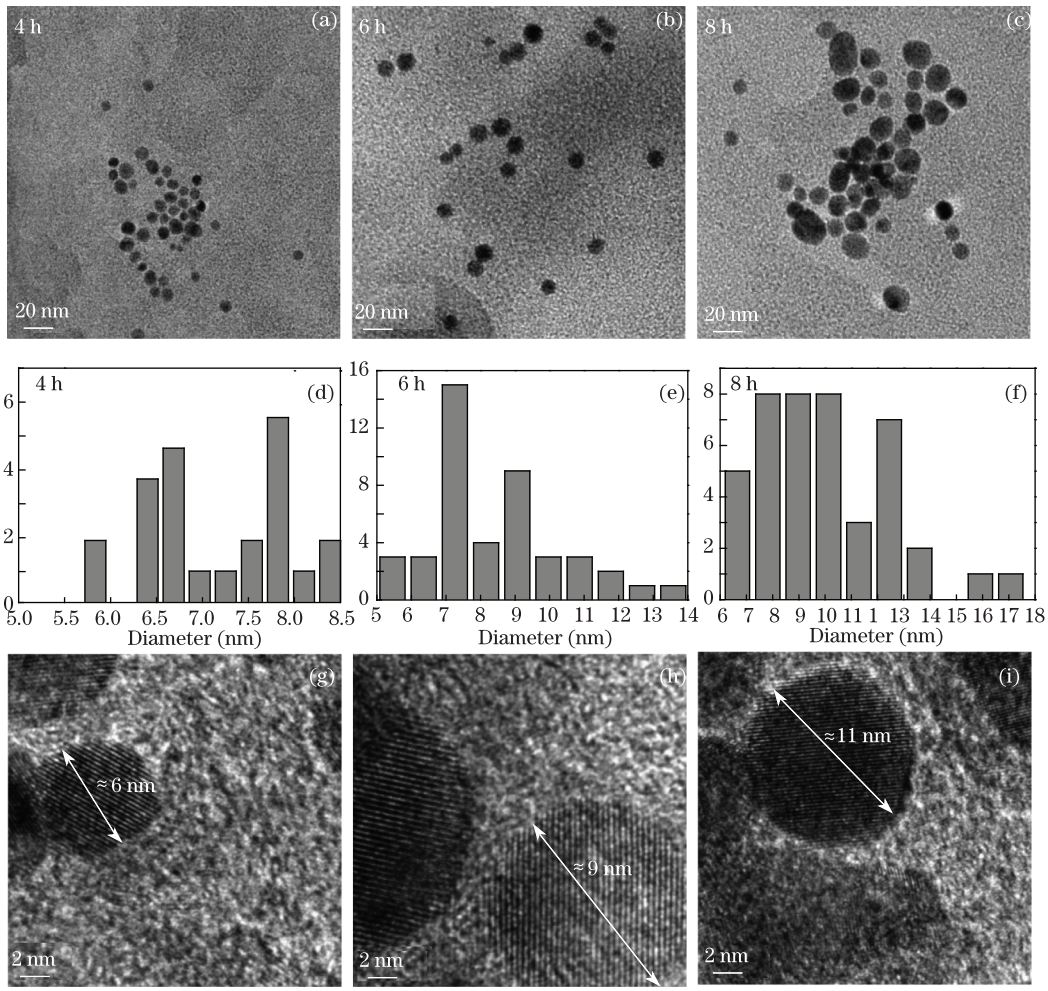

Fig. 5. TEM images of unsupported gold nanoparticles extracted from the amino-functionalized MTFs by a $C_{12}H_{25}SH$/HF/ethanol solution, which have been dipped in the solution of $HAuCl_4$ for (a) 4 h, (b) 6 h, and (c) 8 h; (d)–(f) particle size distributions and (g)–(i) HRTEM images of a single gold nanoparticle corresponding Figs. 4 (a)–(c), respectively.

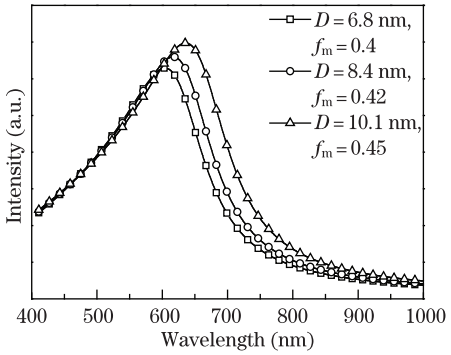

Fig. 6. Simulated extinction spectra of Au/SiO_2 nanocomposites with varying diameters and volume fractions of gold nanoparticles.

and the mean size is about 8.4 nm in Fig. 5(b); the size of the gold nanoparticles ranges from 6.1 to 17.6 nm, while the mean size is about 10.1 nm in Fig. 5(c). These indicate that the size and probably the volume fraction of gold nanoparticles filled in the MTFs increase as dipping time extends. Figures 5(g)–(i) show the HRTEM images of a single gold nanoparticle from the samples shown in Figs. 5(a)–(c), respectively. The sizes of the Au nanoparticles are about 6, 9, and 11 nm, and their d-spacings are all about 0.23 nm indexed to (111), indicating that the gold nanoparticles are well crystallized.

The optical properties of various materials can be described in terms of effective dielectric constants, so that the red shift of the optical absorption peaks of the Au/SiO_2 nanocomposites is caused by the change of their effective dielectric constants, which is brought about by the introduction of gold nanoparticles. The gold nanoparticles are confined within the pore channels in the shape of spheres, and their average size is much smaller than the wavelength of incident radiation. Thus, the extinction properties of the Au/SiO_2 nanocomposite can be analyzed by Maxwell-Garnett (MG) theory[19−21]. In the calculation of the extinction coefficient, we adopted these values relative to gold: the free electron density $N = 5.9\times10^{28}$ m^{-3}, the constant relative to electron-surface interactions $A = 0.43$, the Fermi velocity $v_f = 1.39\times10^6$ m/s, and the bulk damping constant $\gamma_0 = 4.4\times10^{14}$ Hz[22]. The simulated results shown in Fig. 5 indicate that when the size and volume fraction of gold nanoparticles increase, the extinction peaks of Au/SiO_2 nanocomposites shift to longer waves, accompanied by a strengthening of the peak intensity. This is consistent with the experimental results shown in Fig. 4. The dipping time influences the size and volume fraction of the incorporated gold nanoparticles, but the particle size weakly influences the red shift[19,22,23]. The volume fraction may be the primary factor that affects the optical properties of the Au/SiO_2 nanocomposite.

In conclusion, we use Pluronic F127 to synthesize functionalized MTFs, and then assemble gold nanoparticles. TEM, XRD, and spectrometer results show that the well-ordered mesoporous structures are synthesized and the gold nanoparticles are introduced into pore channels and crystallized well. That the SPR absorption peak undergoes a red shift as dipping time extends is analyzed. Both the experimental and simulation results show that extinction peak shifts to longer waves accompanied by intensity-strengthening when the period of neutralization reaction extends, which leads to an increase in the size and volume fraction of gold nanoparticles. We can thus possibly control the optical absorption of the Au/SiO_2 nanocomposite by a simple method, that is, controlling neutralization reaction time.

This work was supported by the Advanced Research Foundation of National University of Defense Technology under Grant No. JC08-02-08.

References

1. H. C. Pfeiffer, R. S. Dhaliwal, S. D. Golladay, S. K. Doran, M. S. Gordon, R. A. Kendall, J. E. Lieberman, D. J. Pinckney, R. J. Quickle, C. F. Robinson, J. D. Rockrohr, W. Stickel, and E. V. Tressler, Proc. SPIE **4343,** 70 (2001).
2. X. C. LeQuan, B. K. Choi, W. P. Kang, and J. L. Davidson, Diam. Relat. Mater. **19,** 252 (2010).
3. U. S. Tandon, Vacuum **43,** 241 (1992).
4. M. Weiser, Nucl. Instrum. Methods Phys. Res. B **267,** 1390 (2009).
5. G. Binning, H. Rohrer, Ch. Gerber, and E. Weibel, Phys. Rev. Lett. **49,** 57 (1982).
6. T. Osada, N. Zhu, Y. F. Zhang, and T. Komeda, J. Phys. Chem. C **112,** 3835 (2008).
7. G. Kwun, E. Jang, G. Kwon, and H. Lee, Curr. Appl. Phys. **9,** 121 (2009).
8. S. Wegscheider, A. Kirsch, J. Mlynek, and G. Krausch, Thin Solid Films **264,** 264 (1995).
9. O. R. Paul, R. Herz, Y.-M. Lin, A. I. Akinwande, S. B. Cronin, and M. S. Dresselhaus, Adv. Funct. Mater. **13,** 631 (2003).
10. G. Fu, W. Cai, C. Kan, C. Li, and L. Zhang, Appl. Phys. Lett. **83,** 36 (2003).
11. R. Mohammadzadegan, H. Mohabatkar, M. H. Sheikhi, A. Safavi, and M. B. Khajouee, Physica E **41,** 142 (2008).
12. H. Fan, K. Yang, D. M. Boye, T. Sigmon, K. J. Malloy, H. Xu, G. P. López, and C. J. Brinker, Science **304,** 567 (2004).
13. A. Fukuoka, H. Araki, Y. Sakamoto, N. Sugimoto, H. Tsukada, Y. Kumai, Y. Akimoto, and M. Ichikawa, Nano Lett. **2,** 793 (2002).
14. J.-L. Gu, J.-L. Shi, G.-J. You, L.-M. Xiong, S.-X. Qian, Z.-L. Hua, and H.-R. Chen, Adv. Mater. **17,** 557 (2005).
15. M.-S. Hu, H.-L. Chen, C.-H. Shen, L.-S. Hong, B.-R. Huang, K.-H. Chen, and L.-C. Chen, Nature Mater. **5,** 102 (2006).
16. Z. Sun, L. Xiao, L. Cao, X. Song, and D. Sun, Chin. Opt. Lett. **7,** 964 (2009).
17. X. Zhang, J. Wang, W. Wu, S. Qian, and Y. Man, Electrochem. Commun. **9,** 2098 (2007).
18. X. Zhang, W. Wu, J. Wang, and X. Tian, Appl. Surface Science **254,** 2893 (2008).
19. R. Ruppin, Opt. Commun. **182,** 273 (2000).
20. G. L. Hornyak, C. J. Patrissi, C. R. Martin, J.-C Valmalette, J. Dutta, and H. Hofmann, NanoStr. Mater. **9,** 575 (1997).
21. C. F. Bohren and D. R. Huffman, *Absorption and Scattering of Light by Small Particles* (Wiley Interscience, New York, 1983).
22. J. H. Hodak, A. Henglein, and G. V. Hartland, J. Chem. Phys. **112,** 5942 (2000).
23. M. Y. Koledintseva, R. E. DuBroff, and R. W. Schwartz, Progress Electromagn. Res. **63,** 223 (2006).